^{15}N Chemical Shift Tensors of β-HMX

Jacalyn S. Clawson,[†] Mark Strohmeier,[†] Dirk Stueber,[†] Anita M. Orendt,[‡] Dewey H. Barich,[†] Blaine Asay,[§] Michael A. Hiskey,[§] Ronald J. Pugmire,[†] and David M. Grant*,[†]

Department of Chemistry and Center for High Performance Computing, University of Utah, Salt Lake City, Utah 84112, and High Explosives Physics Team, High Explosives Science and Technology, Los Alamos National Laboratory, Los Alamos, New Mexico 87545

Received: October 3, 2001; In Final Form: March 29, 2002

The ^{15}N principal values and orientations of the chemical shift tensors of β-HMX are obtained by means of a FIREMAT experiment. A fitting routine using first-order perturbation theory to account for the residual dipolar coupling from neighboring ^{14}N nuclei, responsible for broadening and/or splitting of the ^{15}N resonances, was used to obtain the information from the experimental data. Intermolecular electrostatic interactions are incorporated into nitrogen chemical shielding calculations using several theoretical molecular models. The embedded ion method, a charge model, produced charge densities that improved the correlation between experimental chemical shifts and calculated chemical shieldings by 60% over single-molecule calculations, thus bringing the RMS within anticipated experimental error. The improvements made by the embedded ion method also provided the means to assign the nitrate resonances.

Introduction

Numerous theoretical and experimental studies have attempted to identify factors governing the sensitivity and reactivity of energetic materials. Such systems are complex, involving molecular, crystalline, and physical factors. Solution NMR[1] is one of the techniques that has been used to study energetic materials. Zeman and colleagues[2] have illustrated relationships between liquid-state isotropic chemical shift and explosive characteristics. According to these workers, linear relationships exist for such characteristics as electron spark sensitivity, heat of fusion, activation energy, and detonation velocity. However, solution NMR studies neglect important crystal-lattice effects that are vital in the determination of explosive properties. In addition, many nitramines, $R_1R_2N-NO_2$, demonstrate conformational polymorphism and have crystallographic diversity information which is lost in solution. Solid-state NMR is a sensitive technique for probing molecular and crystal structure as nitrogen-15 NMR is particularly sensitive to intermolecular interactions in the solid state.[3]

In this work we explore the measurement of the ^{15}N chemical shift tensors of energetic materials. The study focuses on nitramines, an important class of energetic materials. This group includes the two most widely applied explosives, octahydro-1,3,5,7-tetranitro-1,3,5,7-tetrazocine (HMX) and 1,3,5-trinitro-1,3,5-triazacyclohexane (RDX), as well as emerging materials such as 2,4,6,8,10,12-hexanitrohexaazaisowurtzitane (HNIW). Solid-state ^{15}N isotropic chemical shifts of HMX and RDX have been acquired from cross polarization magic angle spinning (CP-MAS) spectra.[4] Nitramines exhibit complex solid-state NMR spectra due to the dipolar coupling of the observed spin $^1/_2$ nuclei (^{15}N) with the neighboring quadrupolar ^{14}N nuclei. This coupling, known as the "residual" dipolar coupling, gives rise to line broadening and/or an asymmetric doublet in high-speed CP-MAS spectra. If these effects are not included in the fitting routine, large uncertainties are obtained in the principal values. The spectral effect of the ^{15}N−^{14}N dipolar coupling may be simulated if the nuclear quadrupole moment, the size and orientation of the electric field gradient (EFG) at the ^{14}N nucleus, and the dipolar coupling constant are taken into consideration. Thus, fitting the ^{15}N FIREMAT spectrum provides not only the principal shift values but also the orientational features of these values in the molecular frame.

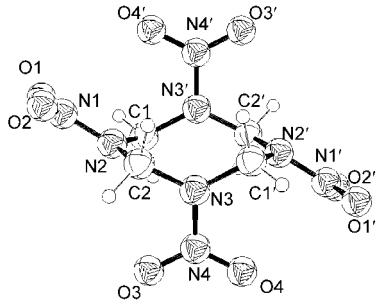

Figure 1. Neutron diffraction structure of β-HMX by Choi et al.[5] The equatorial amine atoms are N2 and N2′, and the axial amine atoms are N3 and N3′.

HMX exists in four polymorphic forms designated as α, β, δ, and γ. The β crystal structure is stable at ambient conditions and is the conventional form used in explosive applications. The β-HMX molecule,[5] shown in Figure 1, exhibits inversion symmetry, with four unique nitrogen positions, two amine and two nitrate positions. The two $N-NO_2$ groups are essentially planar and exist in equatorial and axial conformations. The α-polymorph also has four nitrogen positions resulting from 2-fold crystal symmetry.[6] However, δ-HMX[7] and γ-HMX[8] have no molecular symmetry, and all eight nitrogen positions are either chemically or conformationally distinct. The multiple nitrogen sites and structural sensitivity of ^{15}N chemical shifts provide an opportunity to use ^{15}N solid-state NMR spectroscopy to study the subtle differences present in the HMX polymorphs.

* To whom correspondence should be addressed. E-mail: grant@chem.utah.edu.
[†] Department of Chemistry, University of Utah.
[‡] Center for High Performance Computing, University of Utah.
[§] Los Alamos National Lab.

10.1021/jp013679h CCC: $22.00
Published on Web 06/06/2002

In this paper we report the experimental ^{15}N chemical shift tensors of β-HMX and discuss the theoretical methods necessary to accurately calculate these values.

Experimental Section

Materials. Both a natural abundance and a 10% uniformly labeled ^{15}N sample of β-HMX, prepared by the procedure outlined by Coburn and Ott,[9] were provided by Los Alamos National Laboratory. The polymorphic form was verified by X-ray powder diffraction.

Acquisition of NMR Data. All NMR experiments were performed on a Chemagnetics CMX-400 spectrometer operating at a nitrogen frequency of 40.55 MHz and a proton frequency of 400.12 MHz. The ^{15}N spectra were referenced to glycine at -346.4 ppm on the nitromethane scale. Saturation recovery experiments were performed on both the labeled and unlabeled samples to determine the proton spin$-$lattice relaxation time, T_1. The T_1 data identify a discrepancy between the ^{15}N-enriched sample with a T_1 of 158 ± 7 s and the natural abundance sample with a T_1 of 1180 ± 70 s. The shortened T_1 of the enriched sample is due to the presence of an inorganic free radical, as verified by electron spin resonance. The radical impurity has a g value of 2.28, which is typical of a metal, and is sufficiently removed from a g value of $\sim$2.00 of the NO_2 radicals; this observation is indicative of contamination during labeling rather than decomposition. To verify the isotropic shifts, a slow-spinning (1230 Hz) ^{15}N CP-MAS spectrum was acquired overnight (for safety concerns a high-speed CP-MAS was not attempted). Additional experimental parameters are as follows: contact time of 10 ms, pulse delay of 20 min, and spectral width of 40 kHz. Nitrogen-15 chemical shift principal values and orientations to the molecular frame were obtained by means of a FIREMAT experiment.[10] The FIREMAT spectrum was obtained at 466 Hz, with a pulse delay of 3 min, a 90 ^{1}H pulse width of 4.5 μs, a contact time of 10 ms, a 180 ^{15}N pulse width of 18.6 μs, a spectral width of 44.8 kHz, an acquisition time of 79.3 ms, and 96 scans in each of 16 increments.

Data Processing. The FIREMAT data were fit to a model that includes the quadrupolar and dipolar interactions using the program described by Strohmeier et al.[11] The theoretical basis for the model has been the topic of numerous reviews[12] and will not be reviewed here.

Calculations. Gauge-including atomic orbital (GIAO) chemical shielding calculations[13] were employed using the GAUSSIAN 98 package, with four levels of density functional theory (DFT) and several different basis sets. Two pure density functionals, BLYP[14,15] and BPW91,[14,16] were examined along with B3LYP[15,17] and B3PW91,[16,17] which are hybrids of the Hartree$-$Fock theory and DFT. The basis sets explored were D95 and 6-311G. The necessity for diffuse and/or polarization functions was examined with the D95 basis function at the B3LYP level of theory. The calculated ^{15}N chemical shielding values, σ_{calcd}, were converted to the chemical shift scale by linear correlation to experimental values. The intercept may be compared to the absolute chemical shielding value for nitromethane,[18] -135.8 ppm. A slope of -1 is expected for the linear correlation caused by shift and shielding scales increasing in opposite directions. The neutron diffraction geometry was used for the β-HMX calculations. In addition to calculations on an isolated molecule, calculations incorporating crystal-lattice effects were also performed. The molecular models used to account for these interactions included a cluster model, which added two chemically significant neighbors explicitly into the chemical shielding calculation, and the embedded ion method (EIM),[19] a charge model, which represented neighboring molecules with point charges which reproduce the electrostatic potential. Last, a combined molecular model, where the cluster was embedded within the point charge array, was used.

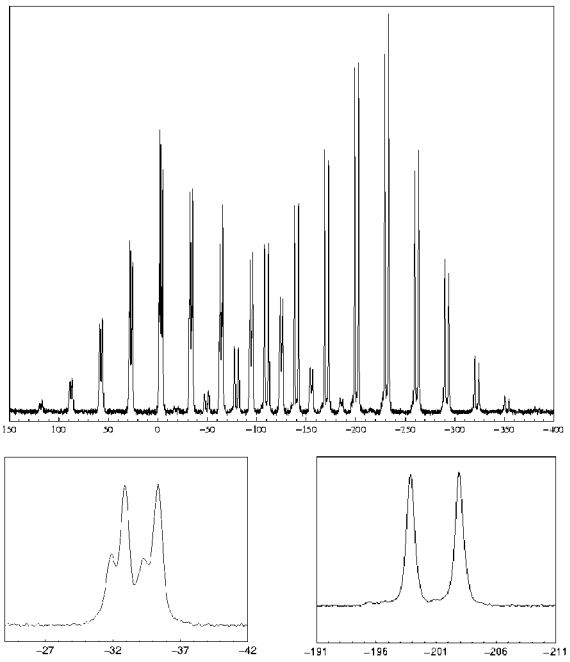

Figure 2. Slow-spinning CP-MAS spectrum of β-HMX. Expansions of the center bands are given at the bottom.

Results and Discussion

Spectroscopic Data. A slow-spinning CP-MAS ^{15}N spectrum of β-HMX obtained at a spinning rate of 1230 Hz is shown in Figure 2. The two amine peaks at -200 ppm are significantly broadened by the residual dipolar coupling to $^{14}NO_2$. However, the magnitude of the EFG tensor is insufficient to produce a well-resolved 2:1 doublet. The ^{15}N nitrate resonances, at ca. -33 ppm, on the other hand, show the characteristic asymmetric doublets of a larger residual dipolar coupling.

The first increment of the FIREMAT spectrum of β-HMX is shown in Figure 3. The chemical shift principal values were determined using the quadrupolar/dipolar-corrected fitting program.[11] The ^{14}N quadrupole coupling constants (χ) and asymmetric parameters (η) were previously acquired by NQR spectroscopy[20] and are given in Table 1. The NQR frequencies of the two amines have been assigned by variable-temperature NQR experiments. Assignments for the nitrates were unavailable. The NQR study also reported that the orientation of the unique EFG tensor axis lies along the N$-$N bond. The initial dipolar coupling constants (D_i) were calculated to be $D_i = 335$ Hz and $D_i = 321$ Hz from eq 1

$$D_i = (\mu_0/4\pi)\gamma_1\gamma_2 h/4\pi^2 r^3 \qquad (1)$$

using neutron diffraction N$-$N bond distances of the equatorial and axial bond lengths of 1.35_4 and 1.37_3 Å, respectively. The experimental values for the dipolar coupling constants were $D_{eq} = 315$ Hz and $D_{ax} = 310$ Hz. The discrepancy was created by thermal motion, which is described elsewhere.[21] Unfortunately, an unequivocal assignment of the ^{15}N resonances based on their residual dipolar splitting could not be made since the exchange of the quadrupole parameters does not sufficiently affect the reliability of the fit. However, assignment of the nitrate

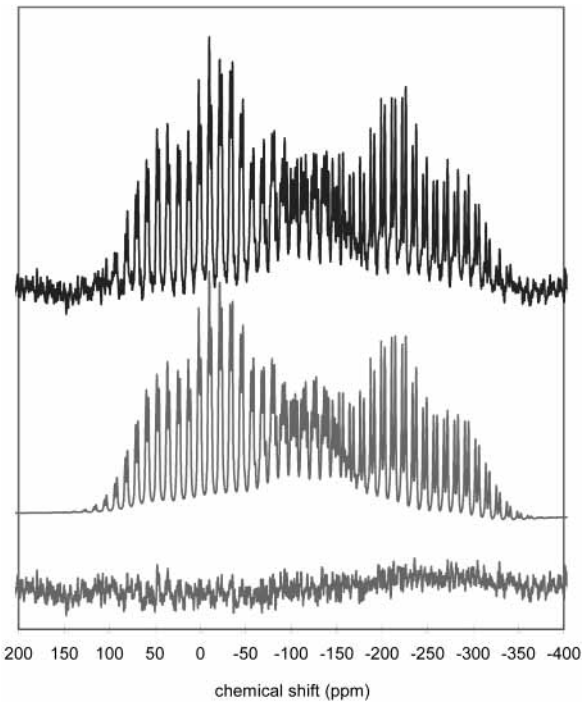

Figure 3. First increment of the ^{15}N FIREMAT spectrum of β-HMX. The upper plot is the experimental spectrum, the middle plot is the best-fit simulated spectrum, and the bottom plot is the residual. Frequencies are on the nitromethane scale.

TABLE 1: Experimental Values of Nuclear Quadrupole Coupling Constants and Asymmetry Parameters for ^{14}N Nuclei in β-HMX[a]

nitrogen type	e^2qQ (MHz)	η	nitrogen type	e^2qQ (MHz)	η
equatorial amine	5.791	0.4977	nitrate	0.840	0.42
axial amine	6.025	0.5189	nitrate	0.806	0.48

[a] Reference 20.

TABLE 2: FIREMAT Experimental ^{15}N Chemical Shift Principal Values for β-HMX

nitrogen type	isotropic shift	δ_{11} (ppm)	δ_{22} (ppm)	δ_{33} (ppm)	span ($\delta_{11-}\delta_{33}$)
equatorial nitrate	−32.7	87	−16	−168	255
axial nitrate	−35.0	92	−32	−166	258
amine	−199.1	−60	−207	−329	269
amine	−203.2	−64	−217	−328	264

resonances was possible on the basis of comparison to calculated chemical shielding values. The experimental results are given in Table 2.

Calculations. The correlations between experimental data and calculated ^{15}N chemical shielding tensor values on an isolated β-HMX molecule are summarized in Table 3. The pairings between experimental chemical shift principal values and theoretical chemical shieldings are consistent for all the correlations. The calculations on the β-HMX molecule illustrate the scatter common to nitrogen chemical shielding calculations on single molecules. The average RMS value and intercept of the correlation improved for the hybrid theories, although no significant difference was observed between the two hybrid theories (Table 3a). As expected, an improvement was achieved when polarization and diffuse functions were added to the D95 basis set (Table 3b). However, the improvements observed with diffuse functions were not substantial enough to warrant the increase in computational time, especially with the intermolecular interaction models. The larger 6-311G** basis set was

TABLE 3: Correlations between Theoretical ^{15}N Chemical Shielding Values of a β-HMX Molecule and Experimental Principal Shift Values

(a) Comparison of Theories on a Single Molecule of β-HMX Using the D95** Basis Set

theory	slope	intercept	RMS[a]
BPW91	−0.85	−91	26
BLYP	−0.86	−98	25
B3PW91	−0.98	−115	17
B3LYP	−0.99	−121	16

(b) Comparison of Basis Sets on a Single Molecule of β-HMX Using the B3LYP Theory

basis set	slope	intercept	RMS[a]
D95	−1.06	−138	23
D95**	−0.99	−121	16
D95^{++}**	−0.99	−124	14
6-311G**	−1.03	−139	17

[a] RMS $= \{(1/(N-2))[\sum(\delta_{exptl} - \delta_{calcd})^2]\}^{1/2}$.

selected for the chemical shielding calculations involving the intermolecular models, since it gave the best pair of RMS value and intercept.

This inability of an isolated molecule model to reproduce experimental chemical shift principal values demonstrates the need for a more robust method for calculating the chemical shift tensor in structures containing large charge polarization and/or intermolecular interactions. It has been shown elsewhere that significant improvements can be made to correlations between experimental and calculated chemical shielding values by including crystal-lattice effects. The crystal-lattice effects have been approximated either by implicitly including significant neighbors into the calculation[22] or by using point charges to simulate the electrostatic potential.[19,23] Both of these approaches were attempted for the β-HMX crystal.

A study by Brill et al.[24] suggested that the important intermolecular Coulombic interactions occur between the axial oxygen (O3) and the axial C1′N3C2 fragment of its neighbor. To a lesser extent, there is an interaction between the equatorial oxygen (O2) and the neighboring equatorial amine (N4) and oxygen (O4) (Figures 5 and 7 in ref 24). Taking advantage of the inversion symmetry within β-HMX, a cluster of three molecules was created where half of the central molecule had the two significant neighbors described by Brill et al. The correlation results and principal values of the chemical shielding tensors using this model are given in Table 4. Some improvement in RMS value (36%) is observed in the cluster chemical shielding principal values over those calculated for the isolated molecule. However, there remain significant errors, primarily in the calculated σ_{11} and σ_{22} values of the nitrates as one can see in Figure 4.

The charge method used to incorporate intermolecular interactions into the β-HMX chemical shielding tensor calculations was originally developed to account for charge interactions in ionic materials.[19] The EIM, described only briefly here, approximates the intermolecular electrostatic interactions inside the crystal. The exact electrostatic potential produced by the field of an infinite ionic crystal lattice can be efficiently calculated by the Ewald summation method.[25] The EWALD program by Klintenberg, Derenzo, and Weber[26] generates a finite point charge array containing a region of defined electrostatic potential. The point charges are calculated using the NBO method[27] as implemented in GAUSSIAN 98. They are situated at the atomic crystallographic sites in the array. The charge array can be broken down into three regions (Figure

TABLE 4: Comparison of the Theoretical ^{15}N Chemical Shielding Principal Values of the Various β-HMX Molecular Models[a]

nitrogen type	principal value	single molec σ_{calcd} (ppm)	cluster σ_{calcd} (ppm)	EIM σ_{calcd} (ppm)	EIM and cluster σ_{calcd} (ppm)	δ_{exptl} (ppm)
equatorial nitrate	σ_{11}	−257	−251	−242	−241	87
	σ_{22}	−93	−111	−125	−125	−16
	σ_{33}	27	28	29	29	−168
axial nitrate	σ_{11}	−243	−241	−232	−234	92
	σ_{22}	−78	−88	−108	−107	−32
	σ_{33}	25	28	28	30	−166
equatorial amine	σ_{11}	−65	−81	−93	−92	−60
	σ_{22}	63	63	63	64	−207
	σ_{33}	207	195	189	187	−329
axial amine	σ_{11}	−73	−82	−91	−91	−64
	σ_{22}	68	69	66	68	−217
	σ_{33}	202	196	189	188	−328
slope		-1.03 ± 0.04	-1.03 ± 0.02	-1.02 ± 0.01	-1.02 ± 0.01	
intercept		-139 ± 7	-143 ± 4	-146 ± 3	-146 ± 3	
RMS[b]		17	11	7	7	

[a] All values were calculated with the B3LYP/6-311G** level of theory. [b] RMS $= \{(1/(N-2))[\sum(\delta_{exptl} - \delta_{calcd})^2]\}^{1/2}$.

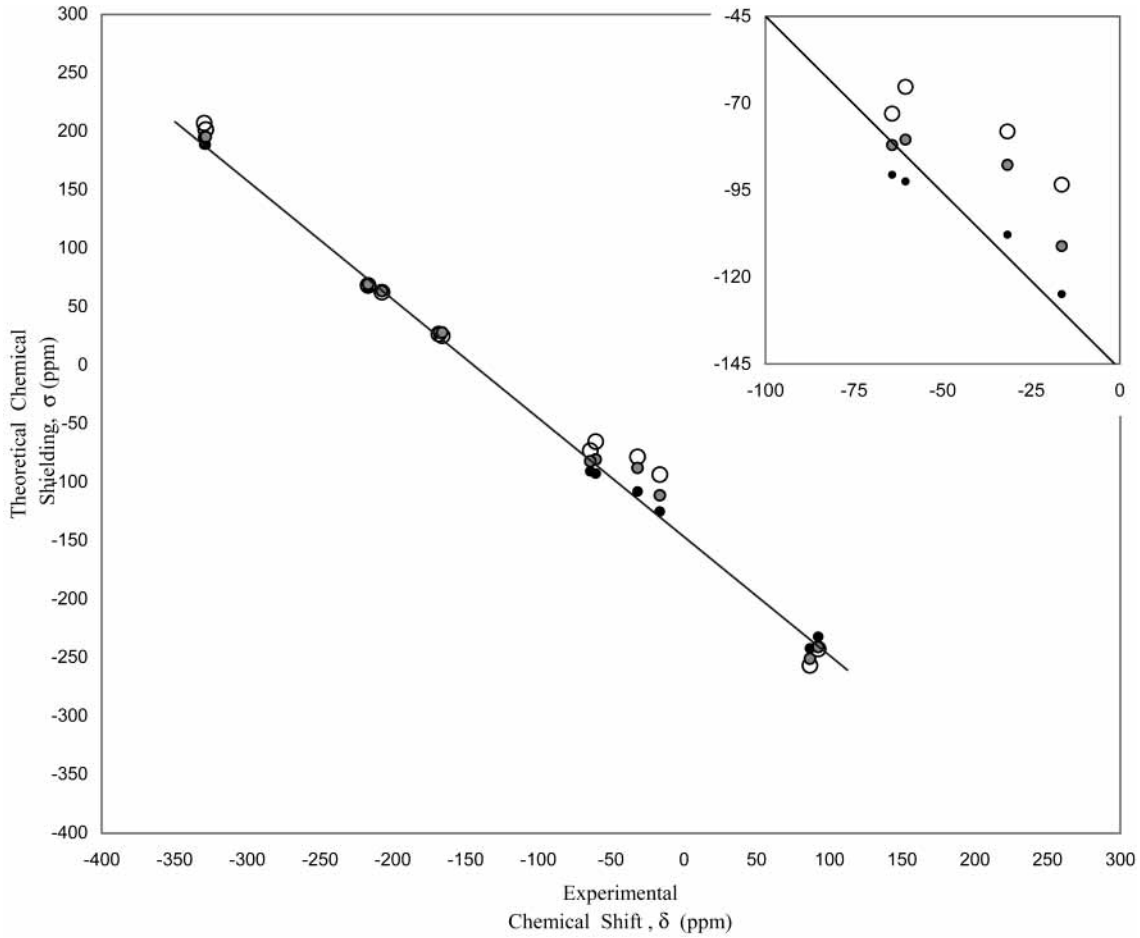

Figure 4. Correlation plot of the theoretical chemical shielding (ppm) versus ^{15}N experimental chemical shift (ppm) on β-HMX. The open circles represent the isolated molecule calculation. The closed gray circles represent the cluster calculation. The black circles represent the EIM results. The regression line from the EIM with slope $= -1.02$, intercept $= -146$ ppm, $R^2 = 0.998$, and RMS $= 7$ is also shown. The nitrate σ_{22} and amine σ_{11} region of the graph is enlarged. All shielding calculations used the B3LYP/6-311G** level of theory.

2 in ref 19). In the outermost region (zone 3), the point charges are varied to establish the electrostatic potential within the quantum cluster, the spherical region near the center of the array. The point charges in the region between zone 3 and the quantum cluster are unchanged and act as a buffer between the varying point charges and the region where the electrostatic potential is defined. After the electrostatic potential has been established, the atoms of the embedded molecule(s) replace the relevant point charges within the quantum cluster. Stueber et al.[19] showed that the EIM significantly improved the results of ^{13}C chemical shift tensor calculations in molecular ionic compounds. The EIM method is not limited to ionic crystals and can be applied to molecular crystals with significant intramolecular charge polarization, as is the case with β-HMX.

Application of the EIM to the β-HMX crystal produced a significant improvement in the correlation between experimental data and calculated ^{15}N chemical shielding tensor values (Table 4 and Figure 4). The RMS value is reduced from 17 ppm for

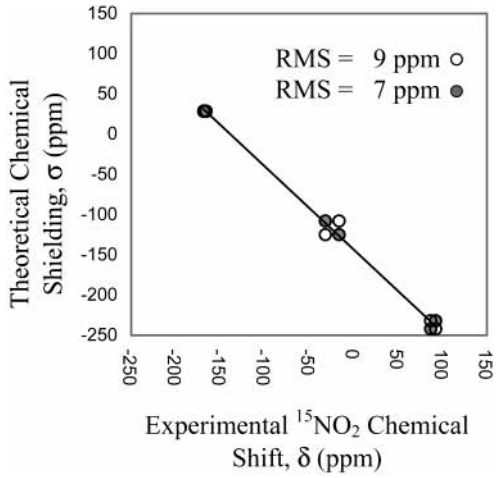

Figure 5. Assignment of the FIREMAT experimental nitrate chemical shifts based on correlations with calculated chemical shieldings from the EIM with B3LYP/6-311G**. Only the nitrate resonances are shown, but all resonances were used for the correlation. The preferred assignment in closed circles has the peak at −32.7 ppm assigned to the nitrate off the equatorial amine and the −35.0 ppm peak assigned to the nitrate off the axial amine. The open circles represent the reverse assignment.

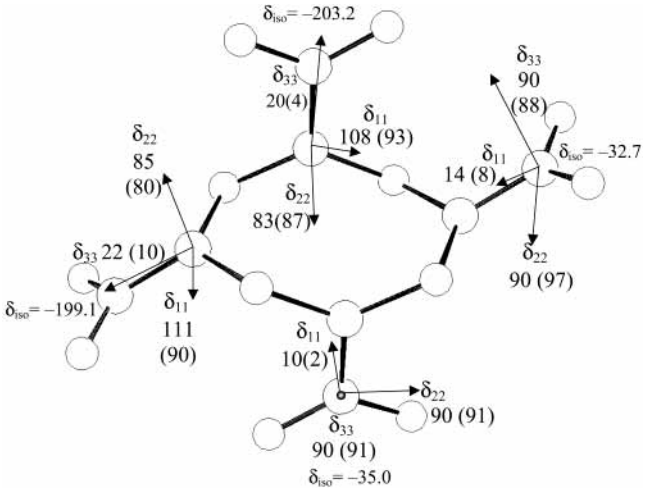

Figure 6. Orientations of the ^{15}N chemical shift principal values in β-HMX. All angles are given in degrees, and the nitrogen atoms are labeled with their isotropic peaks (ppm). Experimental values were determined from the fit of data in Figure 4, and theoretical values, in parentheses, were calculated using the EIM with the B3LYP/6-311G** level of theory.

TABLE 5: NBO Partial Atomic Charges from EIM Calculations on β-HMX Calculated at the B3LYP/D95 Level of Theory**

atom	q_i (initial)	q_f (final)	$q_f - q_i$
C1	−0.036	−0.045	−0.009
H1	0.238	0.273	0.035
H2	0.284	0.286	0.002
N2 (eq)	−0.319	−0.295	−0.024
N1	0.667	0.670	0.003
O1	−0.413	−0.454	−0.041
O2	−0.415	−0.444	−0.029
C2	−0.025	−0.032	−0.007
H3	0.272	0.288	0.014
H4	0.237	0.261	0.024
N3 (ax)	−0.355	−0.326	0.029
N4	0.669	0.689	0.020
O3	−0.409	−0.425	−0.016
O4	−0.395	−0.446	−0.051

an isolated molecule to 7 ppm with the EIM, which is a 60% improvement. The improvements bring the RMS within anticipated experimental error. There was no significant difference between the chemical shielding values calculated by embedding a single molecule or a cluster within the point charge array. This indicates that there are no strong intermolecular interactions that are not well described by the electrostatic potential. The EIM results also permitted clear assignment of the nitrate resonances. If the isotropic peak at −32.7 ppm was to be incorrectly assigned to the axial group, the RMS of the EIM calculation would increase to 9 ppm, a 40% increase in the RMS value over that of the preferred assignment (Figure 5). However, an unequivocal assignment (confidence interval 60%) of the amine resonances could not be made from the EIM calculation.

It is interesting to note the effects that charge polarization can have on theoretical calculations. The experimental value for the relationship of the ^{13}C isotropic chemical shift and fractional charge (q) in electron units equals about 180 ppm/electron.[28] Given the fact that the chemical shift range for the ^{15}N nucleus is approximately 3 times that of the ^{13}C nucleus, one might expect a shift-to-charge relationship on the order of 500 ppm/electron in ^{15}N. Assuming such a relationship is valid, the changes in the charges between the isolated molecule (q_i) and the molecule within the charge array (q_f) (Table 5) would be manifested in shift changes as large as approximately 20 ppm. This high degree of sensitivity to charge polarization seems to correlate nicely with the differences in the RMS errors observed in the various methods of calculation and suggests that the EIM is valid for incorporating intermolecular effects.

In addition to chemical shielding magnitudes, the orientations of the principal values in the molecular frame are also obtained from theoretical fits of the quadrupole-coupled experimental data as well as quantum mechanical calculations. The principal value orientations provide important insight into the electronic structure of the molecule. The orientations for β-HMX are given in Figure 6. The calculated orientations, given in parentheses, were consistent for all calculations regardless of the model, method, or level of theory. The angles given in Figure 6 were calculated with the EIM using the B3LYP/6-311G** level of theory. In the nitrates δ_{11} lies near the N−N bond (lowest π bond order), δ_{22} perpendicular to the N−N bond, and δ_{33} perpendicular to the N−NO_2 plane. This is consistent with the orientations observed for carbon molecules with delocalized π electron systems, such as in aromatics[29] and carbonates.[30] In the case of the amine nitrogen atoms the δ_{33} lies near the N−N bond, δ_{11} is perpendicular to the N−N bond, and δ_{22} is perpendicular to the N−NO_2 plane. The amine orientations are consistent with those previously observed for amide nitrogen.[31] The theoretical orientations agree within experimental error.

The effect of the electrostatic interaction on the principal values depends on the orientation of the components. The components perpendicular to the N−NO_2 plane, the nitrate σ_{33} and amine σ_{22}, are relatively insensitive to electrostatic interactions, with increases to their shielding values of less than 5 ppm, while the nitrate σ_{22} and amine σ_{11} components are significantly deshielded. It is interesting to note that this deshielding effect parallels increased π bonding of the N−N bond, as illustrated by the N−N Wiberg bond orders (Figure 7). In contrast, electrostatic interactions increase the shielding values of the components that lie along the N−N bond. These improvements bring the σ_{22} value of the amines closer to the fitted line. Unfortunately, the σ_{11} value of the nitrates are consistently miscalculated, seemingly reversed from the experimental values. Price[32] suggested that the charge density of lone pair or π electron systems, such as those observed in nitro

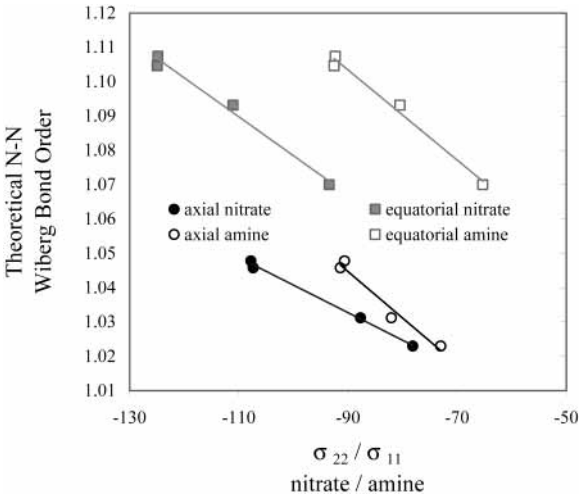

Figure 7. Principal components perpendicular to the N−N bond versus the Wiberg bond order calculated with the B3LYP/6-311G** theory and the EIM.

groups, cannot be accurately represented by monopole expansion of the electrostatic energy (i.e., spherical point charges). The spherical charge distribution assumption made by the EIM may account for the error seen in the σ_{11} component which bisects the NO_2 group.

Conclusion

The ^{15}N chemical shift tensors of the β-HMX molecule have been measured. Incorporation of the quadrupolar and dipolar interactions into the spectral fitting routine was a key factor in the analysis of the experimental data. Significant improvements were observed in the correlations between the theoretical and experimental data using the embedded ion method, bringing the RMS value within the anticipated experimental error. The significant reduction in the RMS value reinforces the earlier report that this method significantly improves theory and experiment correlations, compared to methods that neglect the effect of extensive charge polarization. The shift tensor values may provide additional insights into the electronic and electrostatic lattice properties of β-HMX.

Acknowledgment. The computational resources were provided by the Center for High Performance Computing at the University of Utah. Funding for this project was provided by Los Alamos National Laboratory under Contract F7296-0019-23 and Basic Energy Science of the U.S. Department of Energy under Contract DE-FGO3-94ER14452.

References and Notes

(1) (a) Kaiser, M.; Ditz, B. *29th International Annual Conference of ICT*; Fraunhofer-Institut für Chemische Technologie (ICT): Karlsruhe, Germany, 1998; p 131. (b) Zeman, S.; Mlynarik, V.; Goljer, I.; Dimun, M. Czech. Patent 232 322, 1986. (c) Bulusu, S.; Axenrod, T.; Autera, J. *Org. Magn. Reson.* **1981**, *16*, 52. (d) Farminer, A. R.; Webb, G. A. *Tetrahedron* **1975**, *31*, 1521. (e) Solomon, I. J.; Momii, R. K.; Jarke, F. H.; Kacmarek, A. J.; Raney, J. K.; Adlaf, P. C. *J. Chem. Eng. Data* **1973**, *18*, 335.

(2) (a) Zeman, S. *Propellants, Explos., Pyrotech.* **2000**, *25*, 66. (b) Zeman, S.; Jalový, Z. *Thermochim. Acta* **2000**, *345*, 31. (c) Zeman, S. *Thermochim. Acta* **1999**, *333*, 121. (d) Zeman, S. *J. Energ. Mater.* **1999**, *17*, 305. (e) Zeman, S.; Zeman, V.; Kamenský, Z. *28th International Annual Conference of ICT*; ICT: Karlsruhe, Germany, 1997; p 66/1. (f) Zeman, S. *Thermochim. Acta* **1992**, *202*, 191.

(3) Witanowski, M.; Stefaniak, L.; Webb, G. A. In *Annual Reports on NMR Spectroscopy*; Webb, G. A., Ed.; Academic Press: New York, 1981; Vol. 11B.

(4) Bulusu, S. *31st Sagamore Army Materials Research Conference, Materials Characterization for Systems Performance and Reliability*; Plenum: New York, 1984; p 479.

(5) Choi, C. S.; Boutin, H. P. *Acta Crystallogr.* **1970**, *B26*, 1235.

(6) Cady, H. H.; Larson, A. C.; Cromer, D. T. *Acta Crystallogr.* **1963**, *16*, 617.

(7) Cobbledick, R. E.; Small, R. W. H. *Acta Crystallogr.* **1974**, *B30*, 1918.

(8) Cady, H. H.; Smith, L. C. Report No. LAMS-2652; Los Alamos Scientific Laboratory: Los Alamos, NM, 1962.

(9) Coburn, M. D.; Ott, D. G. *J. Labelled Compd. Radiopharm.* **1980**, *18*, 1423.

(10) Alderman, D. W.; McGeorge, G.; Hu, J. Z.; Pugmire, R. J.; Grant, D. M. *Mol. Phys.* **1998**, *95*, 1113.

(11) Strohmeier, M.; Alderman, D. W.; Grant, D. M. *J. Magn. Reson.*, in press.

(12) (a) McDowell, C. A. In *Encyclopedia of NMR*; Grant, D. M., Harris, R. K., Eds.; Wiley Scientific: Chichester, U.K., 1996; Vol. 5, p 2901. (b) Ernst, R. R.; Bodenhausen, G.; Wokaun, A. *Principles of Nuclear Magnetic Resonance in One and Two Dimensions*; Clarendon Press: Oxford, 1987; p 44.

(13) (a) Ditchfield, R. *Mol. Phys.* **1974,** *27*, 789. (b) Wolinski, K.; Hinton, J. F.; Pulay, P. *J. Am. Chem. Soc.* **1990**, *112*, 8251.

(14) Becke, A. D. *Phys. Rev. A* **1988**, *38*, 3098.

(15) Lee, C.; Yang, W.; Parr, R. G. *Phys. Rev. B: Condens. Matter* **1988**, *37*, 785.

(16) Perdew, J. P.; Burke, K.; Wang, Y. *Phys. Rev. B: Condens. Matter* **1996**, *54*, 16533.

(17) Becke, A. D. *J. Chem. Phys.* **1993**, *98*, 5648.

(18) Jameson, C. J.; Mason, J. In *Multinuclear NMR*; Mason, J.; Ed.; Plenum Press: New York, 1987; p 56.

(19) Stueber, D.; Guenneau, F. N.; Grant, D. M. *J. Chem. Phys.* **2001**, *114*, 9236.

(20) Landers, A. G.; Brill, T. B.; Marino, R. A. *J. Phys. Chem.* **1981**, *85*, 2618.

(21) Zilm, K. W.; Grant, D. M. *J. Am. Chem. Soc.* **1981**, *103*, 2913.

(22) (a) van Alsenoy, C. *J. Comput. Chem.* **1988**, *9*, 620. (b) van Alsenoy, C.; Peeters, J. *J. Mol. Struct.* **1993**, *286*, 19. (c) Peeters, A.; van Alsenoy, C.; Lenstra, A. T. H.,; Geise, H. J. *J. Chem. Phys.* **1995**, *103*, 6608.

(23) (a) de Dios, A. C.; Oldfield, E. *Chem. Phys. Lett.* **1993**, *205*, 108. (b) de Dios, A. C.; Laws. D. D.; Oldfield, E. *J. Am. Chem. Soc.* **1994**, *116*, 7784 and references therein.

(24) Brill, T. B.; Reese, C. O. *J. Phys. Chem.* **1980**, *84*, 1376.

(25) Ewald, P. P. *Ann. Phys.* **1921**, *64*, 253.

(26) Derenzo, S. E.; Klintenberg, M. K.; Weber, M. J. *J. Chem. Phys.* **2000**, *112*, 2074. (b) Klintenberg, M. K.; Derenzo, S. E.; Weber, M. J. *Comput. Phys. Commun.* **2000**, *131*, 120.

(27) Foster, J. P.; Weinhold, F. *J. Am. Chem. Soc.* **1980**, *102*, 7211. (b) Reed, A. E.; Weinhold, F. *J. Chem. Phys.* **1983**, *78*, 4066. (c) Reed, A. E.; Weinstock, R. B.; Weinhold, F. *J. Chem. Phys.* **1985**, *83*, 735.

(28) Spiesecke, H.; Schneider, W. G. *Tetrahedron Lett.* **1961**, 468.

(29) Facelli, J. C.; Grant, D. M. *Theor. Chim. Acta* **1987**, *71*, 277.

(30) Stueber, D.; Orendt, A. M.; Facelli, J. C.; Parry, R. W.; Grant, D. M. *Solid State Nucl. Magn. Reson.*, in press.

(31) Lumsden, M. D.; Wasylishen, R. E.; Eichele, K.; Schindler, M.; Penner, G. H.; Power, W. P.; Curtis, R. D. *J. Am. Chem. Soc.* **1994**, *116*, 1403.

(32) Price, S. L. *J. Chem. Soc., Faraday Trans.* **1996**, *92*, 2997.